Measuring crack growth and related opening and closing stresses using continuous potential drop recording

van Kuijk, Jesse J.A.; Alderliesten, René C.; Benedictus, Rinze

DOI
10.1016/j.engfracmech.2021.107841

Publication date
2021

Document Version
Final published version

Published in
Engineering Fracture Mechanics

Engineering Fracture Mechanics 252 (2021) 107841

Contents lists available at ScienceDirect

Engineering Fracture Mechanics

journal homepage: www.elsevier.com/locate/engfracmech

Measuring crack growth and related opening and closing stresses using continuous potential drop recording

Jesse J.A. van Kuijk *, René C. Alderliesten, Rinze Benedictus

Structural Integrity & Composites, Faculty of Aerospace Engineering, TU Delft, Kluyverweg 1, 2629 HS, Delft, The Netherlands

ARTICLE INFO

Keywords:
Potential drop
Crack closure
Poisson effect
Piezoresistivity
Plasticity

ABSTRACT

To improve resolution of in-situ measurement of crack closure and opening in fatigue, potential drop (PD) measurement technique has been further developed to measure thousands of times through each load cycle with high precision. The results are interpreted with physical phenomena like strain, Poisson's effect, piezo-resistivity, plasticity, and crack growth. Application of the technique to fatigue crack growth tests on aluminum 2024-T3 CCT specimens at different maximum stresses and stress ratios, demonstrate that indeed variations in PD can be associated to development of plasticity and crack opening and closure. Hence, the technique allows to measure timing and magnitude of crack opening and closure stresses in-situ in fatigue crack growth experiments.

1. Introduction

Fatigue crack growth of long cracks in metal alloys can be described using linear elastic fracture mechanics (LEFM). It is often expressed as the crack growth rate da/dN versus a similitude parameter ΔK, function of crack length a and maximum stress $S_{\max}$, or ΔK_{eff}, which is a function of the crack length a, maximum stress $S_{\max}$, and stress ratio R. Measurement of the crack length is generally performed using in situ observations of the specimen surface [1], or using a clip gauge to measure specimen compliance. Crack length measurements can also be performed using the potential drop (PD) technique [2–8], which measures the electrical potential over the remaining cross-section area of the crack plane in metal or other electrical conductive materials, and relates this analytically to the average crack length.

ASTM International provides the E 647 standard [9] on usage of the technique for compact tension C(T), middle tension M(T), and eccentrically-loaded single edge crack tension ESE(T) specimen types since 1978. Compared to (manual) photograph analysis, PD can be measured at each individual cycle which generates larger data sets, to which smoothing and averaging techniques can be applied, resulting in crack length and crack growth rate data of higher resolution and better quality. Furthermore, PD gives a significantly improved estimate of the mean crack progression as it measures the conductive area along the crack plane, rather than only the crack length on the specimen surface.

Most crack growth literature discusses phenomenological approaches and results, based on measurements and simulations. Many theoretical models of plasticity and crack opening and closure share the same limitation: the related (similitude) parameters are expressed per full cycle, implicitly assuming that changes per cycle are instantaneous or averaged over the cycle; d/dN. In reality, crack growth and plasticity development do not occur instantaneously and are dependent on the applied load throughout the cycle. This dependency can be expressed as function $f(d/dt)$, where t is either the real time, or a fictitious, nondimensional time where a cycle runs from $t = 0$ to $t = 1$. The latter option has the advantage of decoupling the observed signal changes from the applied

* Corresponding author.
E-mail address: J.J.A.vanKuijk-1@tudelft.nl (J.J.A. van Kuijk).

https://doi.org/10.1016/j.engfracmech.2021.107841
Received 10 October 2020; Received in revised form 5 February 2021; Accepted 9 June 2021
Available online 16 June 2021

Nomenclature

β	finite width correction factor [-]
ε	strain [-]
ΔK	similitude parameter [MPa $m^{0.5}$]
ΔK_{eff}	similitude parameter [MPa $m^{0.5}$]
Ω	electrical resistance [Ohm]
ν	Poisson's ratio [-]
ρ	electrical resistivity [Ohm m]
σ	standard deviation [-]
ϕ	electrical potential [V]
A	area, specimen cross-section [m^2]
A^*	unit area [-]
CCT	center crack tension specimen type [-]
C(T)	compact tension specimen type [-]
DIC	digital image correlation [-]
E	stiffness [MPa]
EMF	(thermal) electromotive force [-]
ESE(T)	eccentrically-loaded single edge specimen type [-]
FPGA	field-programmable gate array [-]
I	electrical current [A]
L	length [mm]
L^*	unit length [-]
LEFM	linear elastic fracture mechanics [-]
LT	long transverse, material grain direction [-]
M(T)	middle tension specimen type [-]
OL	overload [MPa], [-]
PD	potential drop [-]
PD TTC	potential drop through the cycle [-]
R	stress ratio [-]
S	mechanical stress [MPa]
S_{cl}	closure stress [MPa]
$S_{cl_{phen}}$	closure stress used in ΔK_{eff} equation [MPa]
$S_{cl_{phys}}$	true closure stress [MPa]
S_{max}	maximum stress [MPa]
S_{min}	minimum stress [MPa]
S_{op}	opening stress [MPa]
$S_{op_{phen}}$	opening stress used in ΔK_{eff} equation [MPa]
$S_{op_{phys}}$	true opening stress [MPa]
S_{yield}	yield stress [MPa]
TTC	through the cycle [-]
V	specimen volume [mm^3]
V^*	unit volume [-]
W	specimen width [mm]
a	crack length [mm]
da/dN	crack growth rate [mm/cycle]
h	temperature [deg Celsius]
t	time, fractional time through cycle [s], [-]

test frequency, and is the time definition used in this paper. Fatigue phenomena are generally not time dependent [1], except for secondary effects like creep or corrosion which tend to be orders of magnitude smaller. Integrating the aforementioned function over one full cycle results in a value belonging to that specific cycle:

$$\int_{t_N}^{t_{N+1}} f\left(\frac{d}{dt}\right) dt = \left[\frac{d}{dN}\right]_N \tag{1}$$

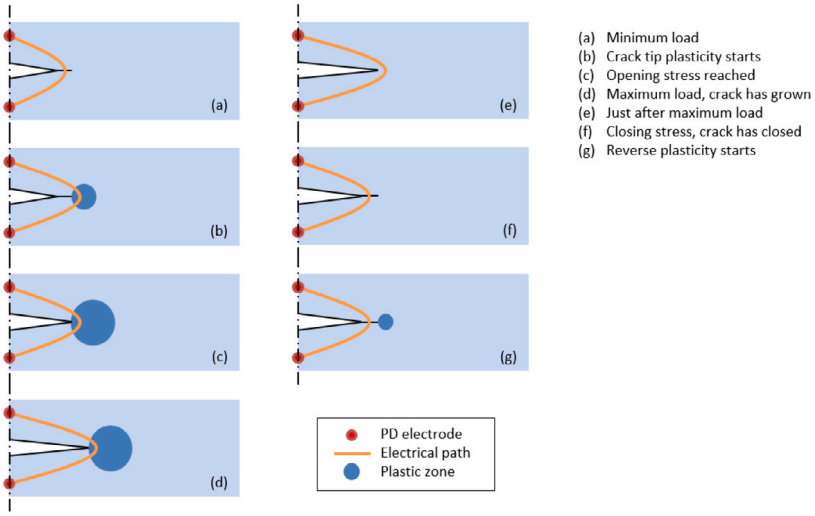

Fig. 1. Schematic view of the PD measurement electric path through a fatigue specimen, at several stages during a fatigue cycle. The applied current flows vertically in each stage.

If fatigue phenomena such as crack growth and plasticity are observable with the potential drop technique, their behavior and development can be tracked during each cycle using multiple potential drop measurements per cycle. Such a measurement system was developed for this study, and is called: potential drop through the cycle, or PD TTC.

Fig. 1 illustrates several different stages during a fatigue cycle, the associated plasticity, and electrical path length. It is clear that the measurement path length is affected, and that it traverses plastically deformed regions which vary in size during a cycle. A standard PD setup takes high frequency measurement(s) at S_{max} only during each cycle (stage (d) in Fig. 1) to prevent closure effects from interfering with the potential measurement, and is therefore unable to capture these effects. The difference in the signal over a period of one cycle (stage (d) to stage (d) in Fig. 1) relates to the crack growth rate da/dN found with standard PD measurements.

The PD TTC setup can perform several hundred to several thousand measurements during each cycle. This high frequency measurement rate throughout the full S range and improved resolution allow for observing the development of the potential through each cycle, creating the opportunity to study the development of plasticity and crack growth within each cycle. This idea is further developed in this paper.

2. Crack opening and closure: the added value of potential drop through the cycle

Elber [10] introduced the concept of crack opening and closure: the crack is open only during part of the cycle, and closed during the other part. Of the different sources reported for this crack tip opening and closure (plasticity, roughness, asperity, etc.) the current work focuses on plasticity induced crack closure and opening, which is generally considered the dominant source.

The related similitude parameter ΔK_{eff} is supposed to incorporate the closure effect and thereby removing the stress ratio effect R, as improvement over the ΔK similitude parameter. Based on this assumption, the closure concept has led to multiple crack closure models such as [1,10–15] which are phenomenologically derived, and validated for various metals, alloys, and R ranges. This closure-based ΔK_{eff} concept is an improvement but not fully successful, given discussions in literature [16–23]. This is partly due to the actual opening and closure happening over a certain range of loading and time [10,24], rather than being instantaneous, and there is some uncertainty regarding the definition of opening and closure [1].

Part of this uncertainty is due to measurement techniques. Crack opening and closure is generally measured using the crack opening displacement (COD) technique. The basic concept is a strain gauge applied in loading direction over the center of the crack, or over the very crack tip, to measure how the local strain changes with the globally applied loading. A change of the slope in this correlation signals the occurrence of opening or closure, but the method is not precise in observing the exact strain and load where the slope becomes constant [1,10,24]. One of the reasons is that the physical gauge locations are influenced by plastic deformation, while this effect is neither accounted for nor corrected for in the COD technique. Convention states that crack opening S_{op} occurs when the crack tip first becomes fully open. Similarly, crack closure S_{cl} happens when the crack tip first starts to close. Schijve [25] states that the values of S_{op} and S_{cl} are generally found to be sufficiently close enough, that S_{op} is used for the closure corrections and the ΔK_{eff} parameter.

It is possible to measure the potential change during crack opening and crack closure with a PD technique, because it will observe changes in potential when the crack length changes. Since these events are connected with the growth of the plastic zone at the crack tip, development of this zone might affect the signal too. From Fig. 1 it can be inferred that the change in potential $d\phi$ within a cycle might not be linearly related to the instantaneous crack extension da. This leads to the hypothesis that measurements from a potential drop through the cycle (PD TTC) technique can be used to relate energy dissipation events such as crack growth and

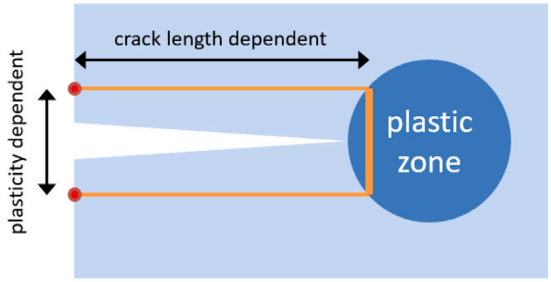

Fig. 2. Schematic view of a fatigue specimen with a crack (one half of a CCT specimen). Crack tip plasticity is present. The effective PD TTC measurement electric path around the crack is shown in orange, connecting the two red electrodes. The current flows vertically through the specimen.

crack tip plasticity development, as well as true crack opening and true crack closure, to specific time intervals and time instants within a fatigue cycle.

Crack opening and closure can be studied in greater detail using PD TTC. In earlier work [26], the authors pointed out that there is a difference between the physical opening stress $S_{\mathrm{op}_{\mathrm{phys}}}$ and the phenomenological opening stress $S_{\mathrm{op}_{\mathrm{phen}}}$. $S_{\mathrm{op}_{\mathrm{phys}}}$ is the true stress at which the crack tip opens, which is challenging to measure accurately as no measurement devices can measure at the crack tip itself. Only FEA appears to be able to give accurate $S_{\mathrm{op}_{\mathrm{phys}}}$ values. The $S_{\mathrm{op}_{\mathrm{phen}}}$ values are widely used by closure corrections and the ΔK_{eff} approach, but originate from measurements in the vicinity of the crack tip, not directly at it. $S_{\mathrm{op}_{\mathrm{phys}}}$ and $S_{\mathrm{op}_{\mathrm{phen}}}$ can be linked through an energy equivalent area approach [26,27]. PD TTC can indirectly observe the true physical opening stress $S_{\mathrm{op}_{\mathrm{phys}}}$, which can be reworked into a $S_{\mathrm{op}_{\mathrm{phen}}}$ value for existing closure corrections. The same procedure holds for reworking $S_{\mathrm{cl}_{\mathrm{phys}}}$ into $S_{\mathrm{cl}_{\mathrm{phen}}}$.

The PD TTC technique in general measures a potential over a crack in a specimen, and the change of potential is the summation of several effects. These effects are only present during parts of a cycle and with varying magnitude, such as extension of the crack and crack tip plasticity growth. The development of these effects can be analyzed from the potential, and are explained in more depth below, to illustrate the applicability and suitability of the PD TTC technique.

3. Change of potential through one cycle

The measured potential is the result of the constant direct current applied to the specimen and the electrical resistance between the PD electrodes, through Ohm's law:

$$\phi = \Omega I \tag{2}$$

The resistance Ω changes due to the strain resulting from the applied loading, and crack growth. Assume that at any given point in time the electrical situation is constant. The specimen is a conductor of uniform cross-section with a uniform current, such that the resistance can be calculated using Pouillet's law:

$$\Omega = \rho \frac{L}{A} \tag{3}$$

Where the specimen geometry parameters length L and cross-section area A, and the resistivity coefficient ρ relate to the total electrical resistance.

The value of ϕ in Eq. (2) will change when Ω changes, as I is constant. It is this potential that is measured with the PD setup.

Two effects have a major influence on the change of Ω: the Poisson effect, which changes with the geometry of the conductor, and piezoresistivity, which changes the resistivity coefficient. Both effects are explained below, and are both present globally when loading is applied to a specimen. There are also two fatigue crack growth specific effects, which are local subsets of the aforementioned effects: crack tip plasticity, and crack extension. Crack tip plasticity changes the local geometry and increases local strain; it is a combined effect of the Poisson effect and piezoresistivity. Crack growth results in a cross-section area reduction and effective overall stiffness reduction: it relates to the Poisson effect. Furthermore it results in a lengthening of the PD electrical conductive path. A schematic view of the electrical conductive path is presented in Fig. 2, showing how crack growth and plasticity affect the conductivity. The relations between the four effects are shown in Fig. 3, and discussed in more detail further on.

3.1. Poisson Effect

Consider a unit cell of a homogeneous isotropic material. When a mechanical load is applied in one direction, then the geometry will elongate in the loading direction, and contract in the transverse directions. The elongation and contractions are related through the Poisson's ratio ν:

$$\nu = -\frac{d\varepsilon_{\mathrm{transversal}}}{d\varepsilon_{\mathrm{axial}}} \tag{4}$$

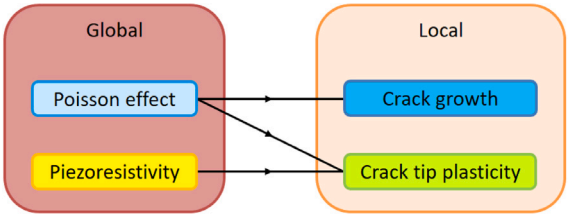

Fig. 3. A schematic view of how the global and local PD effects are related.

For $\nu \neq \frac{1}{2}$ which holds for most materials and metals, a change in strain results in a change in volume. A fatigue specimen acts as a large unit cell, similarly affected by the Poisson effect. When (a part of) the metal specimen is used as an electrical conductor, the geometric changes due to loading will cause a change of electrical resistance over this conductor. A tensile load increases the length between the electrodes, and decreases the cross-section. Both increase the resistance of the conductor.

The change of potential for a given strain can be derived using the following equations. Consider a unit cell of length L^*, cross-section area $A^* = (L^*)^2$, and volume $V^* = (L^*)^3$. Upon an elongation of amount $\Delta L^* = \varepsilon L^*$, resulting in a new length $L^*_{new} = L^* + \Delta L^*$, the ratio of the new volume over the initial volume becomes:

$$\frac{\Delta V^*}{V^*} = \left(1 + \frac{\Delta L^*}{L^*}\right)^{(1-2\nu)} - 1 \tag{5}$$

The new volume then becomes:

$$V^*_{new} = V^* + V^* \frac{\Delta V^*}{V^*} \tag{6}$$

And the new cross-section area follows from:

$$A^*_{new} = \frac{V^*_{new}}{L^*_{new}} \tag{7}$$

Substituting L^*_{new} and A^*_{new} into Eqs. (2) and (3), results in the new electric potential. For a typical value of $\nu = 0.33$ for aluminum 2024-T3 [28], the volume increases when a tensile load is applied. For an electric conductor, not the volume but the length and the cross-section are of importance. In this case, the length increases faster than the volume, and through Eq. (7) the cross-section is found to decrease. Both the increased length and the reduced cross-section result in a higher electric resistance, and thus an increased potential.

3.2. Piezoresistivity

Piezoresistivity is the change in the electrical resistance of a metal when mechanical strain is applied. The resistivity coefficient ρ in Eq. (3) is affected by temperature [29] and mechanical loading [30–35], which both alter the strain on the material. The mechanical loading dependency is of interest here, as most tests are performed at constant temperature. Hunter and Nabarro [30] mention that electrons tend to flow from compressed to expanded regions, meaning that tensile strained regions attract electrons and thus lower the resistivity. This holds for the whole elastically strained specimen, but also for local plastically strained zones such as the crack tip plastic zone. The change is dependent on the crystal structure, and varies therefore with the type of metal and alloy. For typical metal fatigue specimens the effect is observed to be small, less than 0.1% of the total resistivity. For aluminum it holds that the resistance decreases with increasing strain. Morozov et al. [36] show this nonlinear behavior between the strain and the electrical resistance of thin aluminum rectangular strip specimens. Fig. 4 shows this relationship for aluminum 2024-T3 strips for various amounts of plastic strain and for longitudinal and transverse grain directions.

3.3. Crack tip plastic deformation

Consider a fatigue specimen under increasing strain. At the crack tip, a region with $S > S_{\text{yield}}$ exists where plastic deformation occurs. The local strain increases significantly, affecting the local electrical resistivity through the Poisson effect and piezoresistivity. Because plastic deformation happens around the crack tip, it is a very local phenomenon during the majority of the specimen life. The effect on the general dimensions and resistivity of the total specimen are therefore negligible. However, since the PD electrodes are positioned such that the electrical path between them sees a large part of the plastically deformed crack tip region (see Fig. 1), the effect is large enough to significantly influence the resistivity of the PD electrical path. Additional changes in plasticity occur around the crack tip during the crack growth phase as the plastic zone moves along with the crack tip.

It was concluded earlier that the PD TTC curve is proportional to the loading due to the Poisson effect and piezoresistivity. For crack tip plastic deformation it is the piezoresistivity that is affected the most here, making the PD TTC curve depart from the initial proportionality with the loading curve. A similar but smaller discrepancy might be observed near the end of each cycle, where compressive stresses generate reverse plasticity.

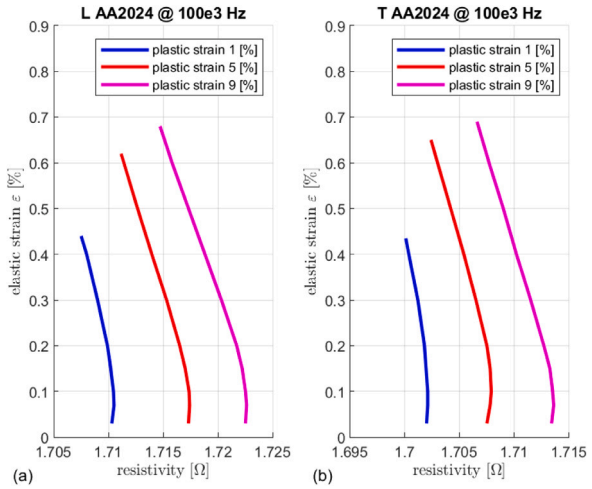

Fig. 4. Piezoresistivity curves for various amounts of plastic strain for aluminum 2024-T3: (a) longitudinal grain, (b) transverse grain. Note initial nonlinearity with increasing strain.
Source: Redrawn from [36].

3.4. Crack growth

The crack growth per cycle is generally small, around nm up to μm for the majority of the crack life as observed in fatigue crack growth tests discussed below. The process of crack opening, extension, and closure during part of the cycle should in theory be observable in the PD TTC signal. The electrical path length increases during crack growth, and the remaining cross-section area of the specimen decreases.

4. Potential drop through the cycle measurement setup

The continuous potential drop measurement system developed in the current study is used to measure the electric potential with high resolution, several orders of magnitude better than required for standard PD. A subset of this data containing the potentials at $S_{\max}$ is used as input for the ASTM method [9] to calculate the crack length a and crack growth rate da/dN. The crack growth rate is plotted versus ΔK_{eff} to generate typical fatigue crack growth curves. The measurement setup and the specimen geometry are discussed separately.

4.1. PD TTC measurement setup

A dedicated PD measurement system was developed in-house at Delft University of Technology. The standard PD procedure is to measure the potential at peak load ($S_{\max}$), either by a single measurement or by averaging multiple (high frequency) measurements at or around $S_{\max}$. PD TTC is capable of continuous high frequency measurements at varying S throughout the full load cycle, which result in more information about the potential with respect to the applied load compared to standard PD. The basic design goals of the new system were:

- Measure the potentials over a test and a reference specimen, and calculate the potential ratio needed for the crack growth equation given in the ASTM E 647 standard [9].
- Measure these two potentials simultaneously to reduce data scatter.
- Perform continuous PD measurements at kHz rate for a test frequency up to several Hz for data smoothing.
- Perform continuous PD TTC measurements at kHz rate for a test frequency of several Hz to observe the change in potential through every cycle of a sine signal.
- Automatically track the minima and maxima of the sine spectrum, to find the standard PD potential at $S_{\max}$ for every cycle.

The potential drop measurements and subsequent data operations are handled by an FPGA (field-programmable gate array), here a National Instruments CompactRIO Controller cRIO 9074 [37]. It controls two separate potential measurement circuits, and it can store temperature measurements of ambient air or the specimens using thermocouples. These temperature measurements can be used during post-processing to correct for stiffness changes. PD measurement wires of equal length were used, and were twisted to minimize thermal EMF. The use of the potential ratio between a test and a reference specimen also minimizes thermal EMF by canceling out most temperature effects. A constant current power supply is connected to the specimens to generate the potentials. Most tests use the Delta Elektronika SM100-AR-75, set at 75 A. The electrical resistance of total circuit gives a potential

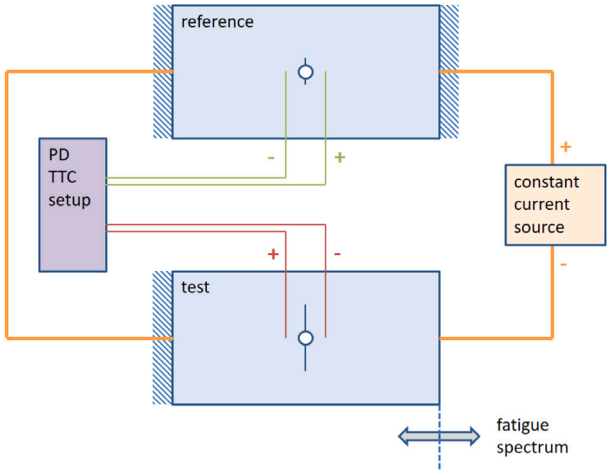

Fig. 5. Schematic view of the test setup with potential drop measurement device and constant current source. Actual tests were performed with a 250 kN MTS fatigue machine.

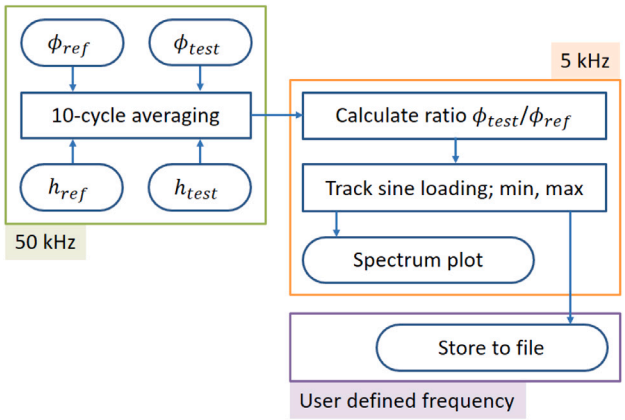

Fig. 6. Potential drop measurement FPGA flow chart.

of about 0.5 V. This results in about 37.5 W of power being supplied to the circuit. This power heats up the specimens until a thermal equilibrium up to 5 °C above ambient is reached, verified by thermocouples. The test is not started before this equilibrium is reached. The complete setup is illustrated in Fig. 5.

The FPGA is programmed using LabVIEW, and the measurement routines are developed in-house at the Delft Aerospace Structures and Materials Laboratory (DASML) of Delft University of Technology. The FPGA is concerned with seven tasks:

- Take simultaneous potential measurements at a frequency of 50 kHz, and apply an averaging function per 10 measurements, resulting in a smoothed signal of 5 kHz.
- Regularly take zero-current potential measurements, for calculating the true potentials.
- Track the test specimen load signal from the fatigue machine as measured by a load cell for sine loading peak–valley detection, to obtain the start and end times of each cycle.
- Calculate the potential ratio used in the ASTM E 647 standard [9].
- Reduce data scatter by using a moving average smoothing over a user-defined number of cycles.
- Measure the temperature of both specimens with thermocouples.
- Write the moving average smoothed measurements of one cycle to a data file every user-defined amount of cycles.

A flow chart of the FPGA software routine is given in Fig. 6.

4.2. Fatigue specimen material and geometry

The test and reference specimens were made as identical copies from the same material batch, of which only the test specimens were fatigued. A typical specimen was CNC milled from 2024-T3 aluminum plate of 6.1 mm thickness. The test specimens were

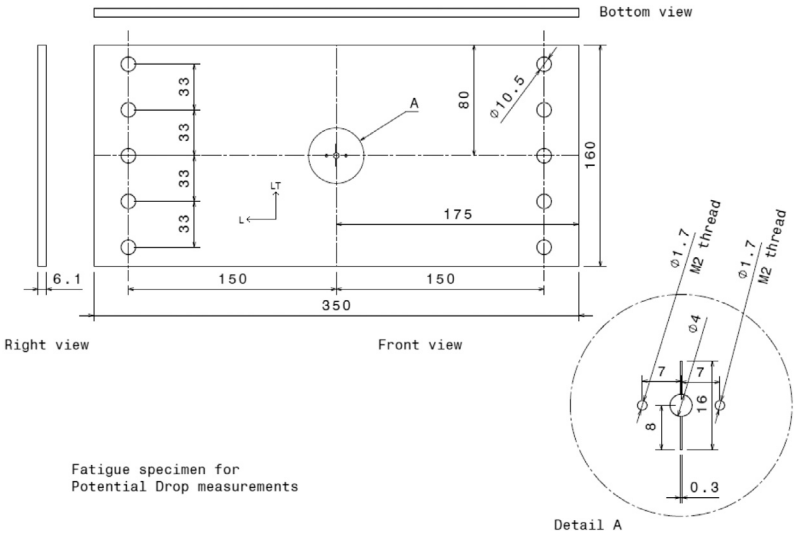

Fig. 7. Drawing of a typical fatigue test specimen as used with the PD TTC setup. Loading direction horizontal. The constant current was connected through the edge holes on the horizontal centerline.

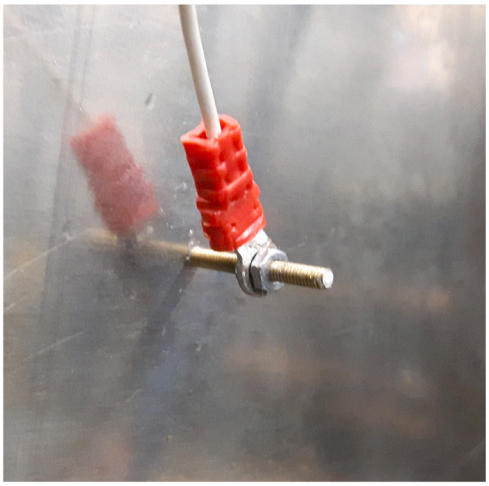

Fig. 8. Close-up of a representative PD electrode attachment. The M2 brass bolt connects the PD wire with the specimen.

loaded in L-T direction, and had on each end five attachment holes of 10.5 mm diameter for clamping. Fig. 7 shows the specimen geometry and location of the PD electrodes. A center hole of 4 mm made it possible to create starter cracks by fretsaw, with $a = 8.0 \pm 0.2$ mm based on visual inspection.

The electrode attachment was similar for all specimens. Two M2 tapped holes were used for attaching M2 brass bolts. Fig. 8 shows a close-up of an electrode attachment. PD measurement wires with appropriate crimp fittings were bolted onto these brass bolts and were not in direct contact with the specimens.

5. PD TTC test results

A number of PD CCT fatigue tests were performed using a constant amplitude spectrum, with and without overloads. The test results are published as data set [38], and Table 1 gives an overview of these tests. Test 8 is a sine spectrum on an uncracked specimen to investigate the potential behavior in absence of crack growth and plasticity. For the other tests it holds that the observed PD TTC curves behave similar for various S_{max} and R values. Test 1 is a representative example used below to illustrate the findings of the PD TTC measurements.

For all tests except test 8, a moving average smoothing of 500 cycles was applied. A PD TTC cycle was stored every 50 or 100 fatigue cycles, resulting in data sets in the order of several hundred PD TTC cycles each. The AFGROW software [39] was used to generate predictions using the NASGRO equation and the material choice of 2024-T3 Al clad, plt & sht, L-T direction.

Table 1
PD TTC tests. Al 2024-T3, CCT fatigue specimens, constant amplitude. Tests 6 and 7 had an overload approximately equal to twice S_{max}. Test 8 is not a fatigue test.

Test no. [-]	S_{max} [MPa]	R [-]	N [cycles]	OL [-]
1	97.06	0.063	24,594	No
2	174.8	0.608	23,534	No
3	145.9	0.607	50,254	No
4	116.6	0.608	1,12,644	No
5	87.4	0.608	3,35,791	No
6	87.8	0.100	48,170	Yes
7	87.8	0.101	44,998	Yes
8	160.0	0.025	–	No

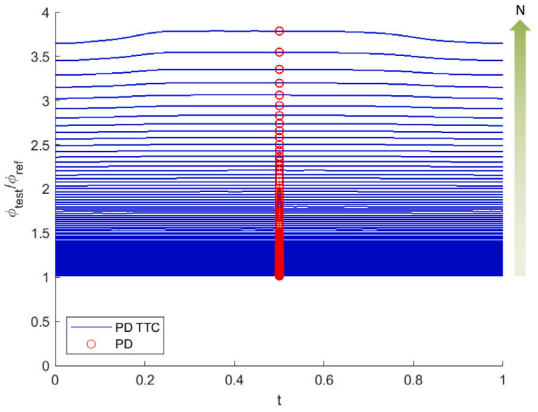

Fig. 9. Potential ratio curves of test 1, per cycle time t. A subset consisting of each 250th curve is shown for clarity. With increasing crack length, the ratio increases. The values at $t = 0.5$ correspond to standard S_{max} PD values.

The differences between both crack growth curves is mostly in the different crack formation lives, as result of the fact that in the tests cracks had to nucleate from the fretsaw cut tip. To compare both crack growth curves, the AFGROW curve is translated to start at nearly the same crack length as the measured curve.

Increasing R and/or lowering S_{max} would result in a longer life at lower da/dN and more PD TTC cycles. However, at lower da/dN the relative precision is less given the measurement resolution, and a larger number of cycles is needed for moving average smoothing. This is discussed in more detail in section Section 6, and a rather short fatigue life test was chosen to increase the relative measurement precision.

The measured PD TTC potentials include the potential ratios of the test and reference specimens. The reference specimen potential was observed to be virtually constant, resulting in the potential ratio being effectively proportional to the test specimen potential. The output files of the measurement device contain the test specimen potential and the potential ratio.

5.1. Standard PD results from PD TTC data set

Using only values at $t = 0.5$ at S_{max}, the crack growth potential ratio per cycle appears which is commonly used as input for the ASTM PD crack length calculation. The results of test 1 are shown below as a representative example. The measured PD TTC ratio is shown in Fig. 9. Each curve starts at a higher potential ratio, because each cycle starts at an increased crack length. The change in potential through a single cycle increases during the specimen life too, and deviations become more pronounced as well.

The values at $t = 0.5$ in Fig. 9 constitute the standard, once per cycle PD measurements. Fig. 10 shows the ASTM PD crack length calculation results of this subset, together with the AFGROW prediction. The AFGROW curve has been slightly translated horizontally to match the measurement curve due to a deviation in crack formation life.

The corresponding crack growth rate da/dN versus ΔK_{eff} is shown in Fig. 11, where a rather linear section (Paris region II) on double logarithmic scales is observed.

This example illustrates that the standard, once per cycle PD data point is only a subset of the full PD TTC signal, and that consequently more information is present in the PD TTC signal.

5.2. A closer look at the PD TTC signal

In order to compare the potential curve shapes from Fig. 9, all the curves are translated in vertical direction to start at zero. Note that they are only translated, not scaled. This translation preserves the relative changes in potential, but not the absolute values.

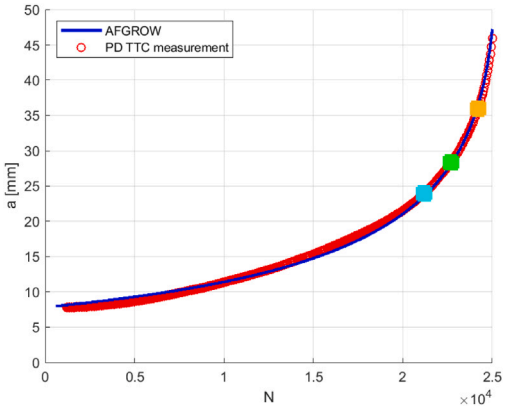

Fig. 10. Crack length versus cycles for test 1. Red data points are generated using the method given in ASTM E647 [9], using the potential values at $t = 0.5$ from the curves shown in Fig. 9. AFGROW curve shown for comparison. The orange, green, and cyan markers correspond with the points in Fig. 11 and curves in Fig. 12.

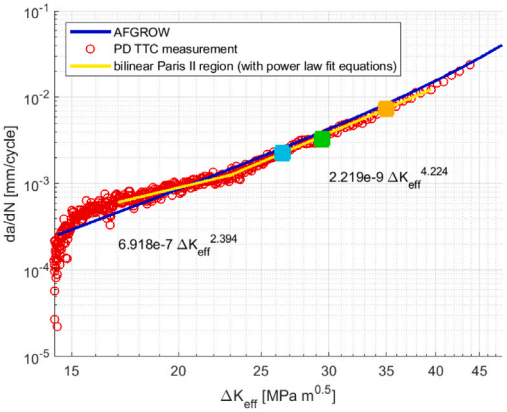

Fig. 11. Crack growth rate curve of test 1. A bilinear Paris region II is observed in the range $17 < \Delta K_{\text{eff}} < 40$. AFGROW curve shown for comparison. The orange, green, and cyan markers correspond with the points in Fig. 10 and curves in Fig. 12.

The result is shown in Fig. 12. Most curves have only a small change in potential throughout the cycle as the largest part of the specimen life at a relatively low da/dN, apparent from Fig. 11, whereas the most pronounced curves are the ones near the end of the specimen life. Nevertheless, Fig. 12 shows that a consistent behavior of the potential is observed throughout a wide range of cycles.

One of the PD TTC curves from Fig. 12 is examined in more detail to explain the behavior of the potential seen in all cycles. In Fig. 13 this curve is overlaid with a sine to show the similarities with the sine loading spectrum. Initially the potential follows this sine behavior very closely. Around one-quarter of the cycle duration does the potential break away into a plateau-like behavior until about three-quarters of the cycle duration. After this plateau, until the end of the cycle, does the potential follow a sine-like behavior again, although not exactly on top of the loading sine.

To give a sense of the plateau significance, the standard deviation of the plateau data range of the green curve from Fig. 12 was calculated. Fig. 14 shows this PD TTC data and the 1σ and 3σ standard deviation boundaries, which encompass 68.2 % and 99.7 % of the plateau data respectively. It is clear that the virtually all plateau data points fall within a small band of potential ratio values, showing that the plateau is a significant feature of the PD TTC curve.

5.3. The origin of the PD TTC plateau

To demonstrate that the observed PD TTC plateau relates to plasticity, a similar but uncracked aluminum 2024-T3 panel was subjected to a low-stress sine loading cycle; test 8. The choice of $S_{\text{max}} = 160\,\text{MPa}$, well below the material yield stress $S_{\text{yield}} = 324\,\text{MPa}$ [28], ascertained absence of any plasticity. With plasticity and crack growth absent, it was expected that the change in potential would be proportional to the change in loading. The observed PD TTC curve closely follows the sine shape, as is shown in Fig. 15. The Poisson and piezoresistivity effects both fluctuate in close accordance with the loading, resulting in the ratio between these effects being rather constant and following the loading signal.

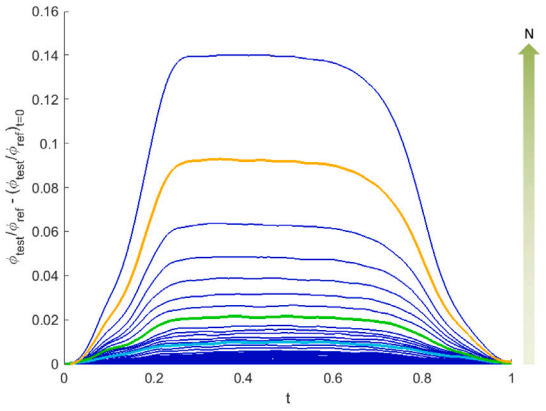

Fig. 12. Potential TTC curves of test 1, per cycle time t. These are the same curves as in Fig. 9, now translated vertically to start from zero to facilitate comparison of the PD TTC curve shape. The orange, green, and cyan curves correspond with the similarly colored points in Figs. 10 and 11.

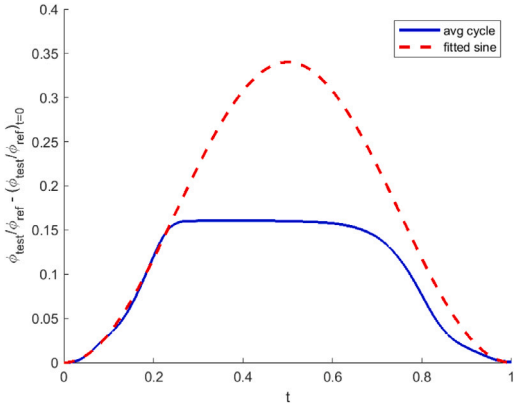

Fig. 13. A single TTC curve from measurements, with an overlaid sine curve representing the applied loading. A correlation is observed during the first and last quarter of the cycle. A plateau appears in between, at a certain load level.

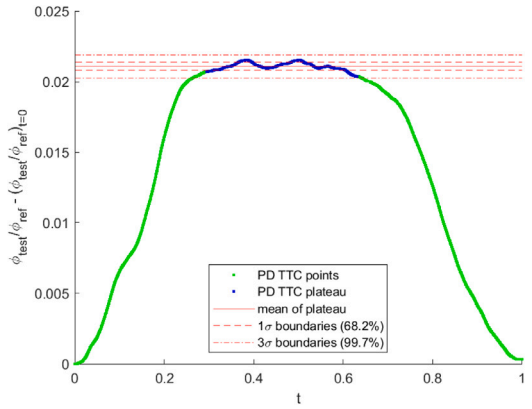

Fig. 14. Potential TTC curve of test 1, corresponding to the green curve in Fig. 12. The plateau data is shown in blue, with 1σ and 3σ standard deviation bands.

A small flattening of the curve is seen directly around $S_{\min}$, which is a result of the initial nonlinearity of the piezoresistivity near zero strain (see Fig. 4). Because the plate does not contain a crack, the change in potential due to elastic loading is small compared to the potential signal of a well developed crack. The relative scatter in Fig. 15 is therefore orders of magnitude larger than the scatter observed in Fig. 13. It also explains the choice for a large $S_{\max}$ compared to the fatigue tests.

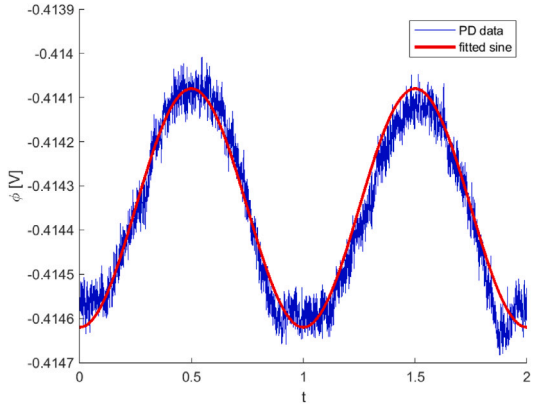

Fig. 15. Two PD TTC cycles from test 8, with an overlaid sine curve representing the applied loading. A clear correlation is observed throughout the cycles. Compare with Fig. 12; the plateau only appears when crack tip plasticity is present.

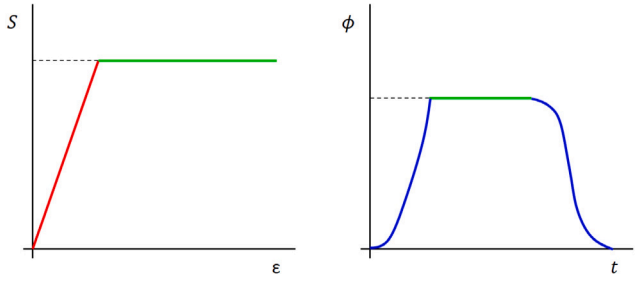

Fig. 16. Elastic perfectly plastic stress–strain curve and corresponding schematic PD TTC curve. Above a certain stress level near or at S_{yield}, plastic deformation exists, which increases ϵ at constant stress and constant potential, resulting in a plateau (green).

A further strengthening of the concept follows from a better understanding of what PD TTC is measuring. This is explained using Fig. 2, where the effective electric path through a part of the specimen is shown schematically. During one cycle, the extension of the crack is small compared to the existing crack. The electric path therefore does not significantly extend in direction of the crack growth (horizontal). During that same cycle the crack tip plastic zone does develop and extend as a result of the applied loading, which is captured by the section of the electric path going around the crack tip (vertical). This shows that the PD TTC signal primarily measures crack tip plasticity. In reality there is not one unique conductive path but rather a conductive field, however the strongest signals are observed near the shortest path. Furthermore it is not a purely geometric function, as the signal strength is also strain dependent and thus a function of plasticity too.

Given the shape of the plastic zone and the electric path, it cannot be directly concluded that the measured signal is linearly proportional with the amount of plasticity. But if the crack tip plasticity is proportional to the total plastic energy dissipation in the plastic zone, then it can be argued that a proportionality exists between the PD TTC signal, the applied load, and the amount of plastic dissipation.

During the plateau phase, there is a difference in potential between the sine loading curve and the plateau level. The sine loading is proportional to the elastic energy present in the global specimen, and the PD TTC signal shows a local effect. Nevertheless, the vertical difference between both in Fig. 13 is a measure for the local energy being dissipated by plastic deformation. The plateau can be explained using an elastic perfectly plastic stress–strain curve, as shown in Fig. 16. Once the local stress reaches a certain level, near or at S_{yield}, the stress stays at this level but the strain increases due to plasticity. It is this effect that causes the PD TTC plateau. In reality there is a slight stress increase during plastic deformation, which accounts for the gradual potential increase at the start of the plateau, and the gradual decrease at the end of the plateau, visually appearing as the rounded corners at the start and end of the plateau.

5.4. Observing S_{op} and S_{cl} with PD TTC

Consider that if the PD TTC curve is related to crack tip plasticity, it also indicates crack growth phenomena such as crack opening and crack closure. As stated earlier, the change in potential due to crack growth itself is too small to be observed with the current measurement setup. However, the change in plasticity behavior can indirectly indicate crack growth effects. This is shown in Fig. 17, based on the curve shown in Fig. 13. The PD TTC curve shows again a sine-like behavior until about one quarter of the cycle length. Here the signal levels off onto the plateau quite abruptly, Fig. 17 shows a short time range around $t = 0.23$ where this

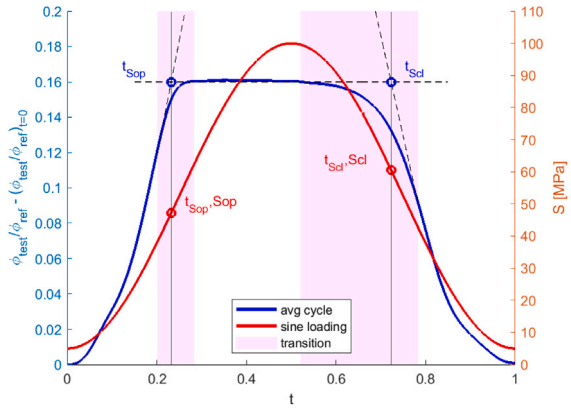

Fig. 17. The plateau region has a nearly constant potential, showing a balanced act between the Poisson effect and the piezoresistivity. Crack opening and closure transition time intervals shown in magenta.

occurs. This range is believed to be the change in global stiffness E as schematically shown in Fig. 18, which occurs when the crack opens and crack growth begins.

The first instant that the PD TTC curve moves away from the sine loading curve proportionality, could be seen as the start of plastic flow. This is the start of the transition phase shown in Fig. 18. Because of the plastic flow, the crack tip is pulled open during the transition point. Residual compressive stresses might be present around the crack tip, originating from previous cycles and depending on the loading conditions. These compressive stresses need to be alleviated first before the crack tip fully opens an crack growth can develop.

In accordance with [16], crack opening was defined as the moment that the crack tip finally becomes completely open. This occurs at the end of the transition phase in Fig. 18, and is the start of the plateau in the PD TTC curve in Fig. 17. Moreover, this point is more easily defined and observed than the start of the transition phase. An analogy can be found in a typical material stress–strain curve. The 0.2 % offset yield point assumption is often used in engineering practice, because the actual elastic limit point is difficult to define accurately.

Noting that opening occurs over a finite time interval, combined with reported [1,10,24] COD measurement scatter of the S_{op} timing, in a similar way the assumption is made that $t_{S_{\mathrm{op}}}$ occurs at the crossing of the tangents at start and end of this opening time interval. This is shown in Fig. 17, from which it is clear that the tangent crossing is easy to determine. S_{op} then follows from the loading curve at $t_{S_{\mathrm{op}}}$.

In a similar way the closing stress S_{cl} can be calculated from $t_{S_{\mathrm{cl}}}$. However, from Fig. 17 it is clear that the time interval during crack closing is significantly larger than during crack opening. The exact reason is yet unknown, but a plausible explanation is that the new crack tip shape after crack extension causes a smooth, gradual closure of this newly formed crack extension. The tangent crossing procedure results in a S_{cl} value slightly higher than S_{op}, which is consistent with literature [25]. This strengthens the idea that the PD TTC concept is capable of deriving indirectly, but rather precise, the load levels at which the crack opens and closes, and how these levels may change throughout the life of the fatigue specimen.

6. Measurement precision and accuracy, signal sensitivity, and smoothing

A brief discussion is given on the sensitivity of PD TTC compared to standard PD, and the application of PD TTC signal smoothing over several successive cycles.

6.1. Measurement precision and accuracy

The measured potentials are in the order of μV, which are amplified by the PD setup to mV. These small signals make the overall electric circuit and measurement setup extremely sensitive to electrical and magnetic interference. The electronic amplifiers must be exceptionally stable to allow for good precision. An improvement in noise reduction is roughly proportional to the improvement of the lower effective da/dN limit. Significant but short-lived potential changes due to local temperature interference have been observed as well, arising from tiny air currents or simply by touching a specimen. The measurement scatter in the amplified mV signal is in the order of mV or smaller, requiring smoothing over multiple cycles.

With the changes in potential through the cycle initially being small, a moving average technique is applied over a constant number of successive cycles. This reduces measurement scatter and improves accuracy. Each measurement point of a given PD TTC cycle is thus the average of a predefined number of previous successive measurements taken at the same PD TTC time instant t. This procedure takes place in the measurement setup FPGA in real time during the test.

The use of this data scatter reduction technique is justified on the basis that for sufficiently small da/dN, it can be assumed that a certain number of subsequent cycles have essentially a constant da/dN at equal a. It appears self-contradictory since a nonzero

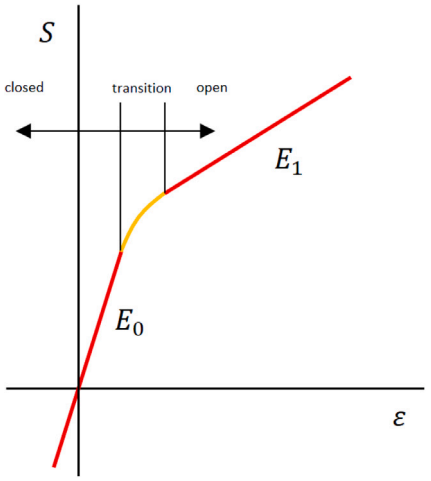

Fig. 18. A schematic, global stress–strain diagram of the specimen belonging to Fig. 17. The nonlinear section (orange) relates to the transition from a closed crack (E_0) to an open crack (E_1, PD TTC plateau).

da/dN results in a change of a, but consider that $da/dN \ll a$. Consecutive PD TTC cycles are thus nearly equal. To further improve measurement precision and accuracy over the current PD TTC setup, electronic amplifiers with less noise ($< 2\,\%$ of absolute signal) and an improved electrical insulation from external disturbances of the whole circuit are paramount.

6.2. PD TTC signal resolution versus standard PD signals

The observed potential changes through the cycle, as indicated in Fig. 1. The presence or absence of plasticity and the occurrence of crack growth influence the signal strength and the signal path length. The ratio of test potential over reference potential generally grows from unity to a value about ten times larger. The change in potential during a single cycle is several orders of magnitude smaller, and is through plasticity and crack growth effects linked to da/dN.

The standard PD technique is a well-established method of observing crack growth during the fatigue life, and generally takes (high frequency) measurements at $S_{\max}$ only. One of the reasons for doing so is that closure effects do not play a role as $S_{\max} > S_{\text{op}}$. The PD TTC technique takes continuous high frequency measurements at varying S values during each full cycle, on purpose measuring how the potential is affected by plasticity and crack growth effects.

With standard PD, the increase in crack length per cycle da/dN is derived from the increase in potential. Measurements are generally taken at only one time instance per cycle, often at $S_{\max}$ at $t = 0.5$. This means that the observed potential increase per cycle is actually the peak to peak value of two successive cycles. A slightly more accurate determination of the potential increase per cycle can be made using the PD TTC data, as the change in potential per cycle can now be properly observed as $d\phi/dN = \phi_{\text{t=1}} - \phi_{\text{t=0}}$, which is directly related to da/dN.

Note that the energy dissipation in plasticity is significantly larger than the energy used to extend the crack. This means for PD TTC that the maximum change in potential through the cycle, equal to $\phi_{\text{t=0.5}} - \phi_{\text{t=0}}$, is orders of magnitude larger than the net change between $\phi_{\text{t=1}}$ and $\phi_{\text{t=0}}$, as is evident from Figs. 9 and 12. Plasticity effects are thus visible using standard PD resolution in this PD TTC setup. In theory, the crack extension within the cycle should be visible too in PD TTC data. However, the current setup has insufficient resolution to do so. Improved resolution (several orders of magnitude) may be required to observe crack extension directly.

6.3. Post-processing data set smoothing

The internal moving average smoothing cannot always provide sufficient relative scatter reduction, especially at PD TTC curves below a certain small da/dN value. A second smoothing step can be performed on the full data set after the test. The chosen method here is smoothing over several successive cycles, centered around a particular N value.

This smoothing range cannot be chosen arbitrarily large, due to three reasons, illustrated in Fig. 19:

1. The relative PD signal scatter is larger at the lower end of the range. The arithmetic mean of the smoothing causes data scatter at the lower end to have a more pronounced effect on the smoothed signal.
2. The monotonous increasing slope of the crack growth rate da/dN makes the higher end of the smoothing range have a stronger effect on the mean or absolute or values of the smoothed PD TTC curve.
3. The growth of a in this range causes the finite width effect to change the increase in plasticity, which affects the PD TTC signal. This effect only becomes significant at large a/W ratios near the end of the specimen life.

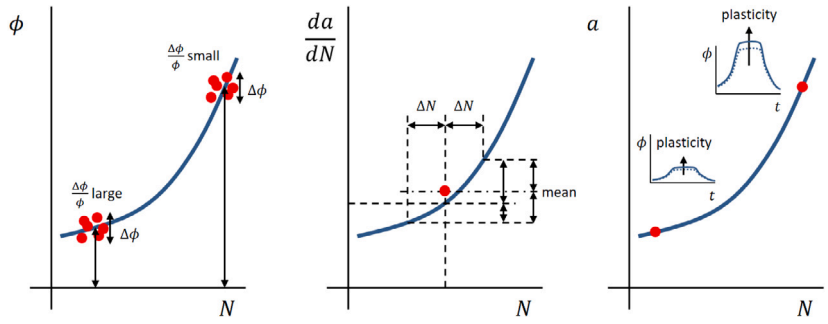

Fig. 19. The three effects of data smoothing and averaging. One: relative scatter versus signal strength. Two: the larger end dominates the symmetric smoothing range. Three: changes in plasticity due to the finite width effect cause the larger end to dominate too, a case unique for PD TTC over standard PD.

While reason 1 and 2 are inherent in data smoothing, and the finite width effect mentioned in reason 3 is always present in fatigue tests, the effect of the latter on plasticity influences the PD TTC curve itself, which is unique to the PD TTC method.

To summarize, the main limitations are that in a given centered smoothing range the lower end increases the overall scatter, while the higher end increases the absolute mean potential.

Based on post-processing of the tests mentioned in Table 1, good results can be obtained by smoothing data sets within certain parameter limits. The ideal post-processing PD TTC curve smoothing needs to be performed on a small data range where:

- The change in da/dN values is sufficiently small (viz. a change up to several %).
- The a/W ratio is sufficiently small (viz. $a/W < 0.125$ such that the finite with correction factor $\beta < 1.05 \approx 1$).
- The da/dN values are such that the relative scatter (unsmoothed) is not too large (viz. up to several %).

The first and second requirement are test geometry and loading dependent, the third requirement is only geometry dependent.

7. Conclusions and recommendations

The extended potential drop (PD) measurement system, PD TTC, is capable of measuring the electric potential throughout a single fatigue crack growth loading cycle, and doing so for many successive cycles. This results in the observation of potential changes which are linked to several crack growth phenomena, such as the timing and magnitude of crack opening and crack closure stresses. The following list summarizes the most important findings of using this PD TTC measurement technique:

1. The known effect of mechanical stress on the electrical resistance is observed in fatigue cycles, affecting the measured potential through Pouillet's law and Ohm's law under assumption of constant current. Two main effects are observed, which have opposite effects on the potential:
   - The Poisson effect: the change of specimen geometry under load. $S \uparrow \propto \phi \uparrow$.
   - Piezoresistivity: the strain dependency of the resistivity. $S \uparrow \propto \phi \downarrow$.
2. During crack growth, two other effects are observed which are subsets of the aforementioned main effects:
   - Crack tip plasticity: changes in strain give a combined effect of the Poisson effect and piezoresistivity.
   - Crack growth: the opening and closing of the crack influences the Poisson effect.
3. Crack tip plasticity and crack growth are readily apparent from a clear deviation of the potential curve around $S_{\max}$. A plateau-like behavior is present at a certain critical cyclic energy level, above which excess energy is dissipated by growth of the crack tip plastic zone and crack growth.
4. The effect of crack extension is several orders of magnitude smaller than plasticity effects, and is therefore not directly observed in PD TTC data given the current measurement resolution. Nevertheless, the observable changes due to plasticity can be correlated with start and end of the crack growth phase.
5. The start and end times $t_{S_{\text{op}}}$, $t_{S_{\text{cl}}}$ of the plateau together with the loading spectrum can be used to derive true opening and closure stresses $S_{\text{op}_{\text{phys}}}$ and $S_{\text{cl}_{\text{phys}}}$, with significantly larger accuracy and precision than existing methods such as COD.

The PD TTC method is novel way of measuring the opening and closing stress with greater insight and potentially improved precision and accuracy over existing methods such as COD. The insights and improvements obtained with PD TTC can be useful in reducing opening and closure stress related uncertainties in ΔK_{eff} similitude parameter models and other crack closure models.

Declaration of competing interest

The authors declare that they have no known competing financial interests or personal relationships that could have appeared to influence the work reported in this paper.

Acknowledgments

This research was carried out under project number S21.5.15581 in the framework of the Partnership Program of the Materials innovation institute M2i (www.m2i.nl) and the Technology Foundation STW (www.stw.nl), which is part of the Netherlands Organisation for Scientific Research (www.nwo.nl). NWO project no. 15012.

References

[1] Schijve J. Fatigue of structures and materials. second ed. Springer Science+Business Media B.V.; 2009.
[2] Baer J. Experimental investigation of short crack growth at notches in 7475-T761. Procedia Struct Integr 2017;5:793–800.
[3] Gajji A, Sasikala G. Potential drop method for online crack length measurement during fracture testing: Development of a correction procedure. Eng Fract Mech 2017;180:148–60.
[4] Gandossi L, Summers SA, Taylor NG, Hurst RC, Hulm BJ, Parker JD. The potential drop method for monitoring crack growth in real components subjected to combined fatigue and creep conditions: application of FE techniques for deriving calibration curves. Int J Press Vessels Pip 2001;78:881–91.
[5] Krompholz K, Ullrich G. Investigations into the fatigue crack initiation and propagation behaviour in Austenitic stainless steel X5CrNi189 (1.4301). Z. Werkst.tech. 1985;16:270–6.
[6] Liu J, Bowen P. DC Potential drop calibration in matrix-cladded Ti MMC specimens with a corner notch. Int J Fatigue 2003;25:671–6.
[7] Scarlin RB. Fatigue crack growth in a cast Ni-base alloy. Mater Sci Eng 1975;21:139–47.
[8] Tumanov AV, Shlyannikov VN, Chandra Kishen JM. An automatic algorithm for mixed mode crack growth rate based on drop potential method. Int J Fatigue 2015;81:227–37.
[9] ASTM Standard Test Method for Measurement of Fatigue Crack Growth Rates. ASTM International E 647-05; 2005.
[10] Elber W. The significance of fatigue crack closure. Damage tolerance in aircraft structures. ASTM STP 1971;486:230–42.
[11] De Koning AU. Crack growth prediction methods, Part 1: a survey. NLR TR 84121 L Part I; 1984.
[12] Newman Jr JC. A crack opening stress equation for fatigue crack growth. Int J Fatigue 1984;24:131–5.
[13] Iwasaki T, Katoh A, Kawahara M. Fatigue crack growth under random loading. Naval Arch Ocean Eng (Japan) 1982;20:194–216.
[14] Kurihara M, Katoh A, Kawahara M. Effects of stress ratio and step loading on fatigue crack propagation ratio. In: Current research on fatigue cracks. London: Current Japanese Materials Research; 1987.
[15] Overbeeke JL, De Back J. The influence of stress relieving and R-ratio on the fatigue of welding joints. In: Maccos SJ, editor. Fatigue of welded constructions. Brighton: The Welding Institute; 1987, p. 11–22.
[16] Vasudevan AK, Sadananda K, Louat N. A review of crack closure, fatigue crack threshold and related phenomena. Mater Sci Eng 1994;A188:1–22.
[17] Vecchio RS, Crompton JS, Hertzberg RW. Anomalous aspects of crack closure. Int J Fatigue 1986;31:R29–33.
[18] Garz RE, James MN. Observations on evaluating fatigue crack closure from compliance traces. Int J Fatigue 1989;11(6):437–40.
[19] Murakami R-I, Kim Y-H, Ferguson WG. The effects of microstructure and fracture surface roughness on near-threshold fatigue crack propagation characteristics of a two-phase cast stainless steel. Int J Fatigue 1991;14(7):741–8.
[20] Okazaki M, McEvily AJ, Tanaka T. The wedge mechanism of fatigue crack growth in silicon nitride. Mater Sci Eng 1991;A143:135–41.
[21] Parida BK, Nicholas T. Effect of stress ratio on fatigue crack growth in a titanium aluminide alloy. Int J Fract 1991;52:R51–4.
[22] Seetharam SA, Dash PK. Load–CMOD data analysis for crack closure. Int J Fract 1992;53:R53–8.
[23] Gómez MP, Ernst H, Vázquez J. On the validity of Elber's results on fatigue crack closure for 2024-T3 aluminum. Int J Fract 1976;12:178–80.
[24] James MN, Knott JF. Critical aspects of the characterization of crack tip closure by compliance techniques. Mater Sci Eng 1985;72:L1–4.
[25] Schijve J. Fatigue crack closure observations and technical significance. In: Report LR-485, faculty of aerospace engineering. Delft University of Technology; 1986.
[26] Van Kuijk JJA, Alderliesten RC, Benedictus R. Unraveling the myth of closure corrections: sharpening the definition of opening and closure stresses with an energy approach. Int J Fatigue 2021;143:106016.
[27] Alderliesten RC. The explanation of stress ratio effect and crack opening corrections for fatigue crack growth in metallic materials. Adv Mater Res 2014;891–892:289–94.
[28] Federal Aviation Administration. Metallic Materials Properties Development and Standardization (MMPDS-05); 2010.
[29] Bloch F. Über Die quantenmechanik der elektronen in kristallgittern. Z Phys 1929;52(7–8):555–600.
[30] Hunter SC, Nabarro FRN. The propagation of electrons in a strained metallic lattice. Proc R Soc Lond Ser A Math Phys Sci 1953;1143(220):542–61.
[31] Kuczynski GC. Effect of elastic strain on the electrical resistance of metals. Phys Rev 1954;92(1):61–4.
[32] Druyvesteyn MJ. The variation of the resistivity of some metals with elastic deformation. Physica 1951;17(8):748–60.
[33] Mackenzie JK, Sondheimer EH. The theory of the change in the conductivity of metals produced by cold work. Phys Rev 1950;77(2):264–70.
[34] Koehler JS. A calculation of the changes in the conductivity of metals produced by cold-work. Phys Rev 1949;75(1):106–17.
[35] Bridgman PW. The effect of homogeneous mechanical stress on the electrical resistance of crystals. Phys Rev 1932;42(6):858–63.
[36] Morozov M, Tian GY, Withers PJ. Elastic and plastic strain effects on eddy current response of aluminium alloys. Nondestruct Test Eval 2013;28(4):300–12.
[37] National Instruments. NI cRIO-9072/9073/9074. User manual and specifications. https://www.ni.com/pdf/manuals/374639f.pdf. [Accessed 5 December 2019].
[38] Van Kuijk JJA, Alderliesten RC, Benedictus R. Data underlying the research on: Al 2024-T3 center crack tension constant amplitude fatigue tests with potential drop through the cycle measurements. http://dx.doi.org/10.4121/12993911.
[39] Harter J. AFGROW user guide and technical manual. AFGROW Fracture Mechanics and Fatigue Crack Growth Analysis software tool. Version 4.12.15.0 Lex Tech, Inc; 2008.